JOURNAL OF GEOPHYSICAL RESEARCH, VOL. 111, A12303, doi:10.1029/2006JA011949, 2006

Climatologies of nighttime upper thermospheric winds measured by ground-based Fabry-Perot interferometers during geomagnetically quiet conditions: 2. High-latitude circulation and interplanetary magnetic field dependence

J. T. Emmert,[1] G. Hernandez,[2] M. J. Jarvis,[3] R. J. Niciejewski,[4] D. P. Sipler,[5] and S. Vennerstrom[6]

Received 30 June 2006; revised 24 August 2006; accepted 21 September 2006; published 1 December 2006.

[1] We analyze upper thermospheric (~250 km) nighttime horizontal neutral wind patterns, during geomagnetically quiet ($Kp < 3$) conditions, over the following locations: South Pole (90°S), Halley (76°S, 27°W), Millstone Hill (43°N, 72°W), Søndre Strømfjord (67°N, 51°W), and Thule (77°N, 68°W). We examine the wind patterns as a function of magnetic local time and latitude, solar cycle, day of year, and the dawn-dusk and north-south components of the interplanetary magnetic field (IMF B_y and B_z). In magnetic coordinates, the quiet time high-latitude wind patterns are dominated by antisunward flow over the polar cap, with wind speeds that generally increase with increasing solar extreme ultraviolet (EUV) irradiation. The winds are generally stronger during equinox than during winter, particularly over the South Pole in the direction of eastern longitudes. IMF B_y exerts a strong influence on the wind patterns, particularly in the midnight sector. During winter, B_y positive winds around midnight in the northern (southern) hemisphere are directed more toward the dusk (dawn) sector, compared to corresponding B_y negative winds; this behavior is consistent with the B_y-dependence of statistical ionospheric convection patterns. The strength of the wind response to B_y tends to increase with increasing solar EUV irradiation, roughly in proportion to the increased wind speeds. Quiet time B_y effects are detectable at latitudes as low as that of Millstone Hill (magnetic latitude 53°N). Quiet time B_z effects are negligible except over the magnetic polar cap station of Thule.

Citation: Emmert, J. T., G. Hernandez, M. J. Jarvis, R. J. Niciejewski, D. P. Sipler, and S. Vennerstrom (2006), Climatologies of nighttime upper thermospheric winds measured by ground-based Fabry-Perot interferometers during geomagnetically quiet conditions: 2. High-latitude circulation and interplanetary magnetic field dependence, *J. Geophys. Res.*, *111*, A12303, doi:10.1029/2006JA011949.

1. Introduction

[2] In our companion paper [*Emmert et al.*, 2006, hereinafter referred to as Paper 1], we presented empirical climatologies of quiet time ($Kp < 3$) upper thermospheric neutral winds measured by seven ground-based Fabry-Perot interferometers (FPIs), and we described the local solar time, day of year, and solar cycle dependence of these data. In this paper we consider the high-latitude results in more detail and describe the influence of the dawn-dusk component of the interplanetary magnetic field (IMF B_y) on the high-latitude wind patterns.

[3] At high latitudes, thermospheric neutral winds are strongly coupled to the convecting ionosphere [e.g., *Meriwether et al.*, 1973; *Richmond and Matsushita*, 1975; *Mikkelsen and Larsen*, 1983; *McCormac and Smith*, 1984; *Rees et al.*, 1986; *Smith et al.*, 1988; *Thayer and Killeen*, 1993; *Richmond et al.*, 2003]. Other momentum sources include pressure gradients caused by Joule heating and heating from solar extreme ultraviolet (EUV) irradiation [e.g., *Roble*, 1995]. Ionospheric convection and Joule heating have strong dependences on the interplanetary magnetic field [e.g., *Heppner*, 1972; *McCormac and Smith*, 1984; *Heppner and Maynard*, 1987; *Weimer*, 2001; *Papitashvili and Rich*, 2002; *Ruohoniemi and Greenwald*, 2005; *McHarg et al.*, 2005], and these depend-

[1]E. O. Hulburt Center for Space Research, U.S. Naval Research Laboratory, Washington, D. C., USA.
[2]Department of Earth and Space Sciences, University of Washington, Seattle, Washington, USA.
[3]British Antarctic Survey, Cambridge, UK.
[4]Space Physics Research Laboratory, University of Michigan, Ann Arbor, Michigan, USA.
[5]Haystack Observatory, Massachusetts Institute of Technology, Westford, Massachusetts, USA.
[6]Danish National Space Center, Copenhagen, Denmark.

0148-0227/06/2006JA011949

ences in turn affect high-latitude neutral wind patterns [e.g., *McCormac and Smith*, 1984; *Killeen et al.*, 1985; *Rees et al.*, 1986; *Meriwether and Shih*, 1987; *Sica et al.*, 1989; *McCormac et al.*, 1991; *Hernandez et al.*, 1991; *Killeen et al.*, 1995; *Richmond et al.*, 2003].

[4] High-latitude thermospheric neutral wind patterns are predominately characterized by a strong antisunward jet over the polar cap, which is driven by EUV-induced pressure gradients and by two-cell ionospheric convection. Under conditions of strong northward IMF, however, the antisunward winds can weaken under the influence of multicellular ion convection and in rare cases turn sunward [*Killeen et al.*, 1985; *McCormac et al.*, 1991; *Niciejewski et al.*, 1994]. During the more common condition of two-cell ionospheric convection, the signature of the dusk cell is observed in the winds, which exhibit a sunward flow on the dusk side, typically around 65° magnetic latitude [e.g., *Thayer et al.*, 1987; *Thayer and Killeen*, 1993]. The influence of the dawn cell on the neutral winds is much weaker [e.g., *Meriwether et al.*, 1973; *McCormac and Smith*, 1984; *Thayer and Killeen*, 1993], and this has been attributed to greater competition from solar-driven pressure gradients and an opposing Coriolis force [*Thayer and Killeen*, 1993; *McCormac and Smith*, 1984].

[5] IMF B_y has been observed to affect the location and orientation of the antisunward wind jet over the polar cap and also the strength of the neutral dusk cell relative to the dawnside wind flow [e.g., *McCormac et al.*, 1985; *Meriwether and Shih*, 1987; *Meriwether et al.*, 1988; *Thayer et al.*, 1987; *Hernandez et al.*, 1991; *Killeen et al.*, 1995]. There is a north-south asymmetry in the effect of B_y on the neutral wind patterns [e.g., *Thayer et al.*, 1987], with northern hemisphere B_y positive conditions producing patterns similar to those of southern hemisphere B_y negative conditions. This north-south difference is readily explained by a similar organization of ionospheric convection patterns [e.g., *Papitashvili and Rich*, 2002] and is ultimately a consequence of geomagnetic field line orientation relative to the IMF [e.g., *Heppner*, 1972].

[6] In this paper we extend the earlier wind results in several ways. The large amount of data we analyze, compared with earlier studies, provides a more refined climatological characterization of wind patterns, particularly in the southern hemisphere. We also present the first side-by-side comparison of northern and southern hemisphere winds under winter conditions, and the first detection of climatological B_y effects on subauroral neutral winds. Our study is fairly unique [see also *Niciejewski et al.*, 1994] in that we study the B_y dependence of the winds under geomagnetically quiet conditions, as represented by the *Kp* index; this restriction may affect the relative importance of ion-neutral momentum coupling, compared to heating-induced pressure gradients. Finally, although earlier studies [e.g., *Hernandez et al.*, 1991] have fit localized wind parameters (such as the peak antisunward wind) as a function if IMF B_y, this is the first attempt to represent average wind patterns continuously as a function of B_y and local time, as well as solar activity.

2. Data and Methodology

[7] Employing the quiet time empirical models developed in Paper 1 from FPI wind data, we analyze high-latitude neutral wind patterns as a function of magnetic local time and latitude, solar EUV irradiance, season, and IMF B_y and B_z (in geocentric solar magnetospheric, or GSM, coordinates). We consider results from the following stations: South Pole (90°S), Halley (76°S, 27°W), Millstone Hill (43°N, 72°W), Søndre Strømfjord (67°N, 51°W), and Thule (77°N, 68°W). Information needed to evaluate the empirical models (in geographic coordinates only) is contained in the auxiliary material for Paper 1. Code for evaluating the models is available from the CEDAR database at http://cedarweb.hao.ucar.edu/tools/empirical_models.html.

[8] As described in Paper 1, only data for which $Kp < 3$ were used. This criterion does not optimally represent quiet conditions at high latitudes, but its simplicity facilitates statistical analysis of the data. Even though *Kp* is not an ideal indicator of high-latitude energy and momentum input, we found that within our quiet time bin the effect of IMF B_z (which is loosely correlated with *Kp*) is generally negligible, except at the polar cap station of Thule (section 3.4).

2.1. Ground-Based IMF Proxies

[9] Direct measurements of IMF provide only intermittent coverage; about 50% of our data have corresponding hourly IMF measurements in the OMNI IMF database maintained by the National Geophysical Data Center http://spidr.ngdc.noaa.gov). This constitutes a statistical impediment to climatological analysis of IMF effects, particularly when analyzed in conjunction with other parameters such as solar EUV irradiance. We therefore use a proxy for IMF B_y and B_z, derived from ground-based magnetometers at Thule and Dumont d'Urville (67°S, 140°E), following the method described by *Vennerstroem et al.* [2001]. The proxy IMF values provide 98% coverage. The regression coefficients for the proxy relationship were computed using 1975–1985 data, a period largely outside of that covered by our wind data, but more recent measurements indicate that the statistical relationship is still valid with a high correlation (0.767) for B_y, as shown in Figure 1, and a slightly lower correlation (0.664) for B_z.

[10] In addition to comparing the space-based IMF measurements directly to the ground-based proxy, we also compared the climatological response of quiet time high-latitude winds to each index. We used quiet time South Pole FPI meridional wind measurements, and first subtracted out the local time, $F_{10.7}$, and seasonal effects represented by the empirical model, to obtain a set of residual winds. We then sorted the residuals into eight 3-hour local solar time bins, three $F_{10.7}$ bins (60–100, 100–175, >175), and the eight look directions (longitudes). For each bin, we computed two linear fits of the residuals: one as a function of OMNI IMF B_y, and the other as a function of the ground-based proxy. The slopes we obtained are shown in Figure 2, with the OMNI IMF slopes plotted on the y-axis, and the ground-based proxy slopes plotted on the x-axis. The correlation of the responses is quite high (0.960), but the magnitude of the response tends to be slightly larger when the ground-based proxy is used, as evidenced by the trend line in Figure 2, which has a slope less than 1. This is consistent with the results of *Richmond et al.* [2003], who found that daytime high-latitude winds are more strongly correlated with the ground-based IMF proxy than with OMNI IMF. As pointed out by *Richmond et al.* [2003], magnetic variations near the

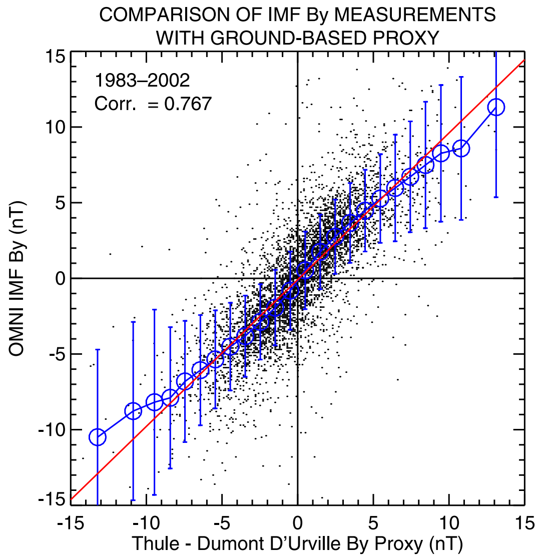

Figure 1. Comparison of hourly OMNI IMF By values (obtained from the National Geophysical Data Center) with proxy values derived (following *Vennerstroem et al.* [2001]) from ground-based magnetometer measurements at Thule, Greenland, and Dumont d'Urville, Antarctica. The blue circles with error bars show average OMNI IMF values for different proxy bins; the bins are 1 nT wide, except for the outer four bins which are 2 and 3 nT wide. The error bars show the standard deviation, and the red line shows a linear fit of the data; the correlation is 0.767. Approximately 95,000 hourly values between 1983 and 2002 were used in the fit, a sample of ~5000 is shown by the black dots.

surface are closely related to ionospheric convection and ion-neutral drag and therefore potentially represent a more sensitive indicator of wind changes.

2.2. Response Time of Winds to IMF Changes

[11] We found that the climatological response of the winds to IMF is broadly maximized at a time lag of 1 hour when the ground-based proxy is used, compared to 1–2 hours with the spaced-based measurements, and this difference is roughly consistent with the propagation time [e.g., *Ridley et al.*, 1998] of IMF changes from the varying locations of the space-based measurements to the ionosphere and thermosphere. We should note that the time delay between space and ground magnetometer measurements was neglected in the generation of the proxy model, but this should not significantly affect the derived statistical relationship between the two time series. *Richmond et al.* [2003] found that daytime winds between 100 and 200 km altitude responded to IMF changes on two broadly defined timescales: 1–4.5 hours and 16–24 hours. Our result of 1 hour is on the low end of the first band; the shorter time lag is possibly attributable to the higher altitudes and nighttime conditions of our data. In any case, our results and those of *Richmond et al.* [2003] both indicate that the exact choice of time lag is not critical. In constructing our empirical models, we used IMF values 1 hour prior to the wind measurements.

2.3. Organization of High-Latitude Winds in Magnetic Coordinates

[12] Thermospheric high-latitude winds are generally better organized in magnetic coordinates than in geographic coordinates, owing to the strong forcing exerted by convecting ions on the neutral constituents. Following *Richmond et al.* [2003], we analyze the winds in quasi-dipole magnetic latitude and magnetic local time [*Richmond*, 1995] coordinates, transforming the wind vectors to their magnetic eastward and magnetic northward components. Figure 3 illustrates, using the South Pole FPI models, the better organization of the winds in this coordinate system, compared to geographic latitude and solar local time. Although solar local time has little intrinsic meaning near the geographic poles, it does serve to organize data that is driven primarily by solar radiation energy inputs. A uniform, antisunward wind flow across the geographic polar cap produces a purely diurnal, longitude-independent variation in the local time dependence of the zonal and meridional components. The fact that the diurnal variation of high-latitude winds shows a strong longitude dependence in geographic coordinates but not in magnetic coordinates indicates that magnetic coordinates facilitate a simpler representation of wind patterns.

2.4. Further Processing of South Pole FPI Winds

[13] As described in Paper 1, the South Pole FPI quiet time empirical models we developed represent meridional winds along each of eight look directions, and we combined model results from neighboring azimuths to estimate the vector wind field over the South Pole. In magnetic coordinates, the results from the different look directions (which represent winds at different geographic longitudes) corre-

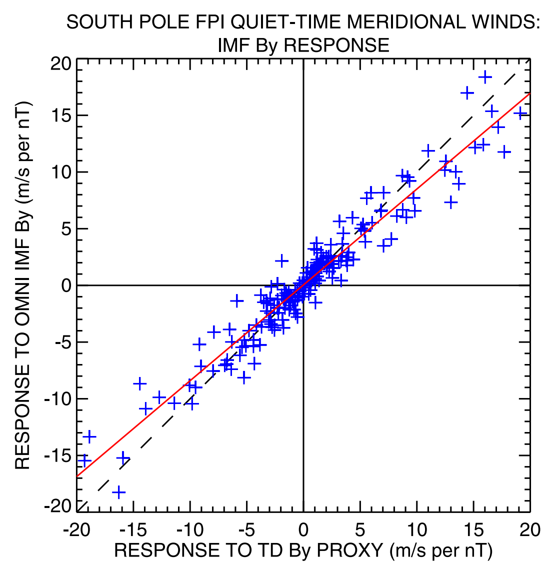

Figure 2. Comparison of the strength of the dependence of quiet time South Pole FPI winds on IMF B_y as measured from space (y-axis) versus IMF B_y inferred from ground-based magnetometers (x-axis). Each symbol represents a different longitude/local time/$F_{10.7}$ bin (a total of $8 \times 8 \times 3 = 192$ bins); the location of a symbol along the x or y axis indicates the linear dependence of the wind data in that bin to the B_y values (also see Figure 7). The solid red line shows the results of a linear fit to the symbols, and the dashed black line is the line of perfect agreement. The fact that the slope of the red line is less than one suggests that the wind measurements are slightly better organized by the ground-based IMF proxy.

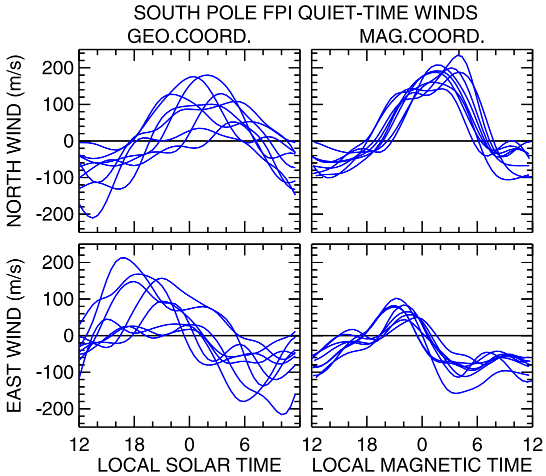

Figure 3. South Pole FPI average quiet time winds as a function of local time in (left) geographic and (right) geomagnetic coordinates. The vector winds were derived from empirical models of meridional winds measured along eight look directions (equivalent to eight different longitudes); the meridional component is shown in the top panels, and the zonal component is shown in the bottom panels. Each curve shows results from a different longitude.

spond to different magnetic latitudes. The top panel of Figure 4 shows the vector winds from each geographic longitude. The magnetic latitudes of these results fall roughly into four values: 71°, 73°, 75°, and 77°. The results for each latitude ring are generally very similar for the two corresponding geographic longitudes, and we therefore averaged them together to obtain the wind field shown in the bottom panel of Figure 4. Table 1 gives the geographic longitudes and magnetic latitudes of the original locations of the vector winds, as well as the average magnetic latitude of each pair. In subsequent figures depicting the South Pole FPI vector wind fields, we only show results from the lowest and highest magnetic latitudes (70.9° and 77.4°).

3. Results and Discussion

3.1. Overall Pattern, $F_{10.7}$ Effects, and Seasonal Effects

[14] Figure 5 shows the vector wind fields derived from the quiet time FPI measurements at five stations, for winter solstice and IMF $B_y = 0$ conditions. Both the northern and southern hemisphere patterns are dominated by antisunward flow over the polar cap; the outlet of this jet is roughly aligned along the 0100 MLT meridian. On the sunward side, there is a substantial dusk-to-dawn component of the flow. None of the stations shows the strong sunward flow in the dusk sector that marks the return flow of the dusk convection cell, although there is a weak sunward flow in the Søndre Strømfjord (73°N) duskside winds. One possible reason is that return-flow latitudes are not sampled by the stations; under quiet conditions, the return flow has been observed to maximize at 65–70° [e.g., *McCormac et al.*, 1987; *Thayer and Killeen*, 1993]. However, in the southern hemisphere, there is no indication of duskside sunward flow in the South Pole FPI winds at 71°, and at 62°, the Halley winds show a strong antisunward flow in the dusk sector, in stark disagreement with the quiet time patterns, based on summer Dynamics Explorer 2 (DE 2) data, presented by *McCormac et al.* [1987] and *Thayer and Killeen* [1993]. The Halley result may be unique to its longitude (27°W); the pattern is similar (albeit with larger wind speeds) to that of Millstone Hill in the north (56° magnetic), at which latitude the wind forcing is presumably dominated by pressure gradients. However, the South Pole FPI results at 71° are from nearby longitudes (37.5°W and 82.5°W; see Table 1). If there are quiet time sunward average winds in this longitude sector between 62° and 71° magnetic latitude, then they are accompanied by strong latitudinal gradients.

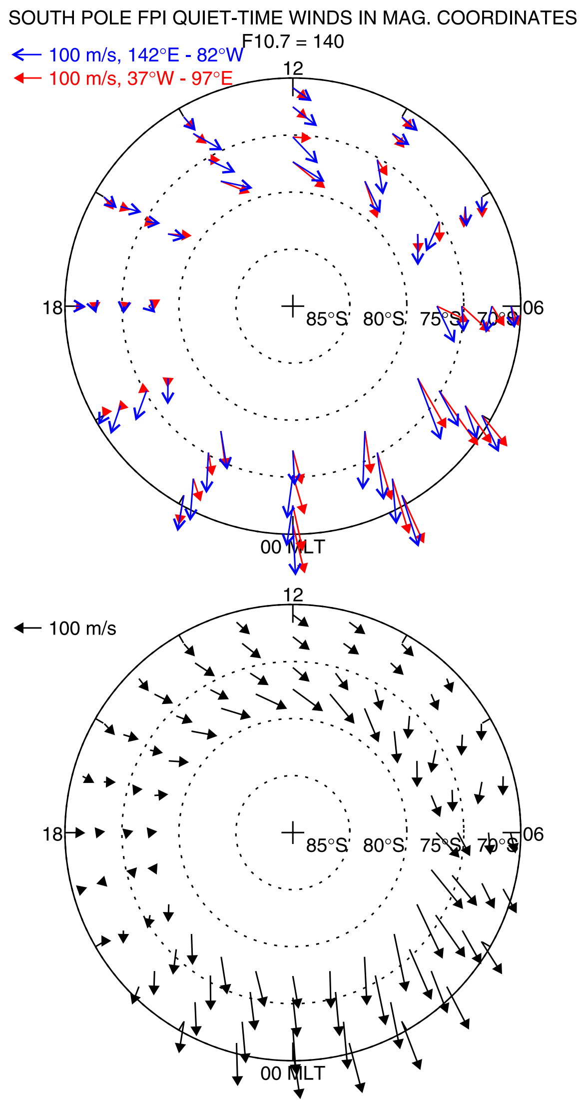

Figure 4. Vector wind fields, for moderate ($F_{10.7}$ = 140) solar EUV conditions during winter solstice, derived from South Pole FPI quiet time wind measurements. The top panel shows vector winds from eight different longitudes: four between 142°E and 82°W (blue) and four between 37°W and 97°E (red). These eight locations fall roughly along four magnetic latitudes (71°, 73°, 75°, and 77°). At each latitude, results from the two longitude sectors are generally very similar, and the bottom panel shows them averaged together.

Table 1. Locations of Derived South Pole Fabry-Perot Interferometer Vector Winds

Geographic Longitude	Geographic Latitude	Magnetic Latitude	Average Magnetic Latitude
82.5°W	86.4°S	71.0°S	70.9°S
37.5°W	86.4°S	70.8°S	
127.5°W	86.4°S	72.8°S	72.5°S
7.5°E	86.4°S	72.2°S	
52.5°E	86.4°S	74.7°S	75.2°S
172.5°W	86.4°S	75.6°S	
97.5°E	86.4°S	77.1°S	77.4°S
142.5°E	86.4°S	77.6°S	

Under disturbed conditions, duskside sunward winds do develop over Halley [*Crickmore*, 1994], so a sharp Kp-dependent convection boundary seems plausible. A longitude-restricted study of southern hemisphere winter DE 2 wind measurements might help to clarify the FPI results.

[15] Figure 5 also shows the effect of $F_{10.7}$ on the wind patterns; results from solar minimum and solar maximum are superimposed. The high-latitude wind magnitudes are consistently larger during solar maximum than solar minimum. The Millstone Hill winds, however, are sharply reduced in magnitude with increasing $F_{10.7}$ (during summer, however, the $F_{10.7}$ dependence is very weak), indicating that there is a transition between a negative $F_{10.7}$ effect at the latitude of Millstone Hill and a positive effect at the latitude of Halley. How sharp this transition is depends on whether it is most strongly organized in geographic or magnetic coordinates; the latitude difference between Millstone Hill and Halley is ~30° geographic and ~6° magnetic. The influence of $F_{10.7}$ on winds at different latitudes is discussed in more detail in Paper 1.

[16] In addition to the $F_{10.7}$ effect on the wind magnitudes, there are also consistent differences in the direction of the wind vectors. On the nightside, between about 2100 and 0300 MLT, the winds (including those at Millstone Hill) tend to be oriented more toward the dusk side during solar maximum (i.e., the winds are more westward). This is possibly a signature of a more influential ionospheric dusk convection cell during solar maximum, compared to solar minimum.

[17] Figure 6 shows some of the effects of season on the wind patterns, under moderate solar EUV conditions (we found the seasonal dependence to be independent of the $F_{10.7}$ dependence, except at Millstone Hill; see Paper 1). For Millstone Hill, winter, spring equinox, and summer conditions are shown; for the higher-latitude stations only winter and equinox are shown. The empirical model for Thule does not contain any seasonal terms (due to poor seasonal coverage), and these winds are attributed to winter conditions. Except at Millstone Hill, the nightside winds tend to be stronger during equinox than winter. This feature is particularly evident in the 77°S South Pole FPI winds (at geographic longitudes of 97.5°E and 142.5°E), where the equinox winds are over twice as strong as the winter winds. This strong seasonal dependence can also be seen in Figure 6 of Paper 1 (note that at this location, noonside solar local times correspond to nightside magnetic local times).

[18] In the midnight sector, the equinox winds tend to be directed more toward the dusk side, compared to winter winds. This effect is not observed in the Halley winds or the 71°S South Pole winds (both of which are located in the Atlantic/American longitude sector).

3.2. IMF B_y Effects

[19] We now examine the linear effect of IMF B_y on the quiet wind patterns. Our analysis of residual winds (after subtracting the modeled local time, $F_{10.7}$, and seasonal effects, as described in section 2.1) as a function of B_y revealed that in most cases, the response is linear, but in a few rare cases, we found nonlinear trends. The B_y response

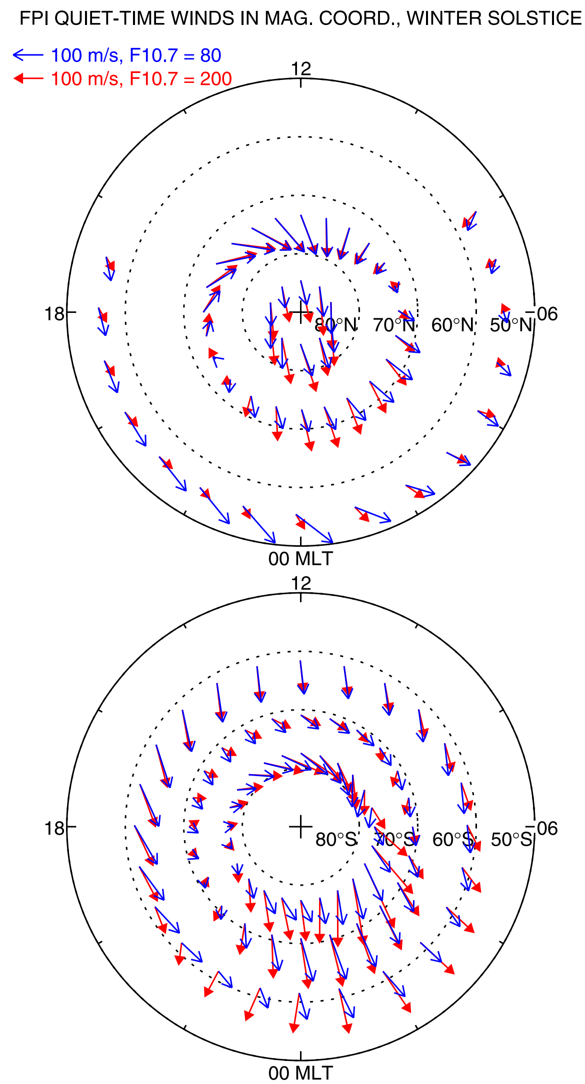

Figure 5. High-latitude quiet time wind fields derived from FPI measurements in the (top) northern and (bottom) southern hemispheres. Results are shown for winter solstice, with low (blue) and high (red) solar EUV conditions superimposed. In the northern hemisphere, the three stations shown are Millstone Hill (outer ring; only north-looking results are shown), Søndre Strømfjord, and Thule (inner ring). In the southern hemisphere, results from two stations are shown: Halley (outer ring) and South Pole (two inner rings). Note that on the sunward side, the Søndre Strømfjord and Halley models are constrained to have no $F_{10.7}$ dependence (due to a relative lack of data near the dayside terminator).

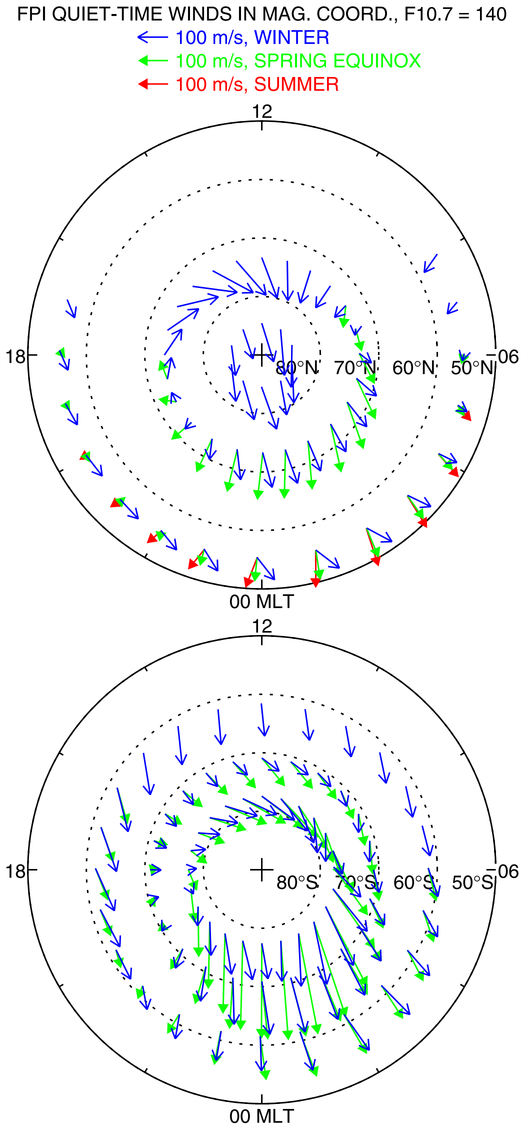

Figure 6. Same as Figure 5, but for moderate solar EUV conditions and with results from different seasons superimposed: winter solstice (day of year 0 in the north, 180 in the south), spring equinox (day of year 80/260) and summer solstice (day of year 180, Millstone Hill only). Arrows are shown only for nighttime conditions (solar zenith angle > 90°).

depends strongly on local time (as expected); we also found that the magnitude of the response tends to increase with increasing $F_{10.7}$, consistent with the results of *Killeen et al.* [1995]. This is illustrated in Figure 7, which shows the response of the South Pole winds as a function of local solar time, with results from different $F_{10.7}$ bins superimposed. These values are the same ones shown along the x-axis of Figure 2. Results from four longitudes are shown; the wind responses at the other four longitudes are very similar in character.

[20] We found the seasonal dependence of the B_y effect to be very weak in general, except at Millstone Hill (see section 3.3), and only the Millstone Hill and Søndre Strømfjord models include coupled B_y and day-of-year terms. The lack of a significant day-of-year effect on the B_y dependence may be a consequence of the limited seasonal coverage of most stations.

[21] Figure 8 summarizes the B_y dependence of the Thule, Søndre Strømfjord, and South Pole quiet time wind patterns. At the lower latitudes (below 75°) shown in the figure, B_y effects are most pronounced in the midnight sector, although it should be noted that the Søndre Strømfjord model is constrained to have no B_y dependence on the dayside (there is a relative lack of Søndre Strømfjord data on the dayside, due to sunlit conditions that occur there even during winter solstice, and we did not find any consistent dayside B_y effects with this dataset). In the northern hemisphere, the nightside B_y negative (B_y-) winds are directed more towards dawn, relative to the B_y positive (B_y+) winds. This behavior is similar to that of the ionospheric convection patterns derived by *Ruohoniemi and Greenwald* [2005] using SuperDARN radar data and by *Papitashvili and Rich* [2002] using DMSP electric field measurements. For neutral-B_z conditions during winter, the results of these studies indicate that the antisunward jet between the dawn and dusk cells is directed toward ~2300 MLT for B_y+ and toward ~0100 MLT for B_y- conditions.

[22] In the southern hemisphere winter, B_y has the opposite effect, with the B_y+ nightside winds being directed more

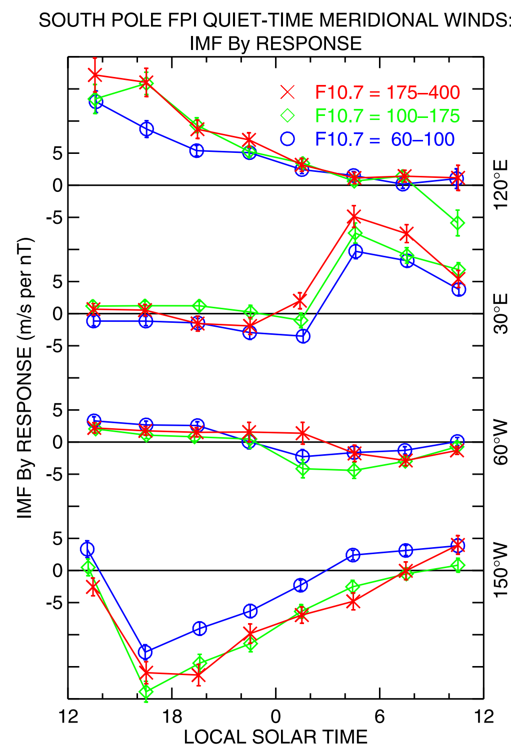

Figure 7. Response of South Pole FPI quiet time meridional wind measurements to changes in IMF B_y (as represented by the ground-based proxy described in the text), as a function of solar local time. Meridional wind data from each look direction (longitude), and from different $F_{10.7}$ and 3-hour local time bins, were linearly fit to IMF B_y (after removing local time, $F_{10.7}$ and seasonal effects). Shown here are the slopes of the fits from four of the eight longitudes.

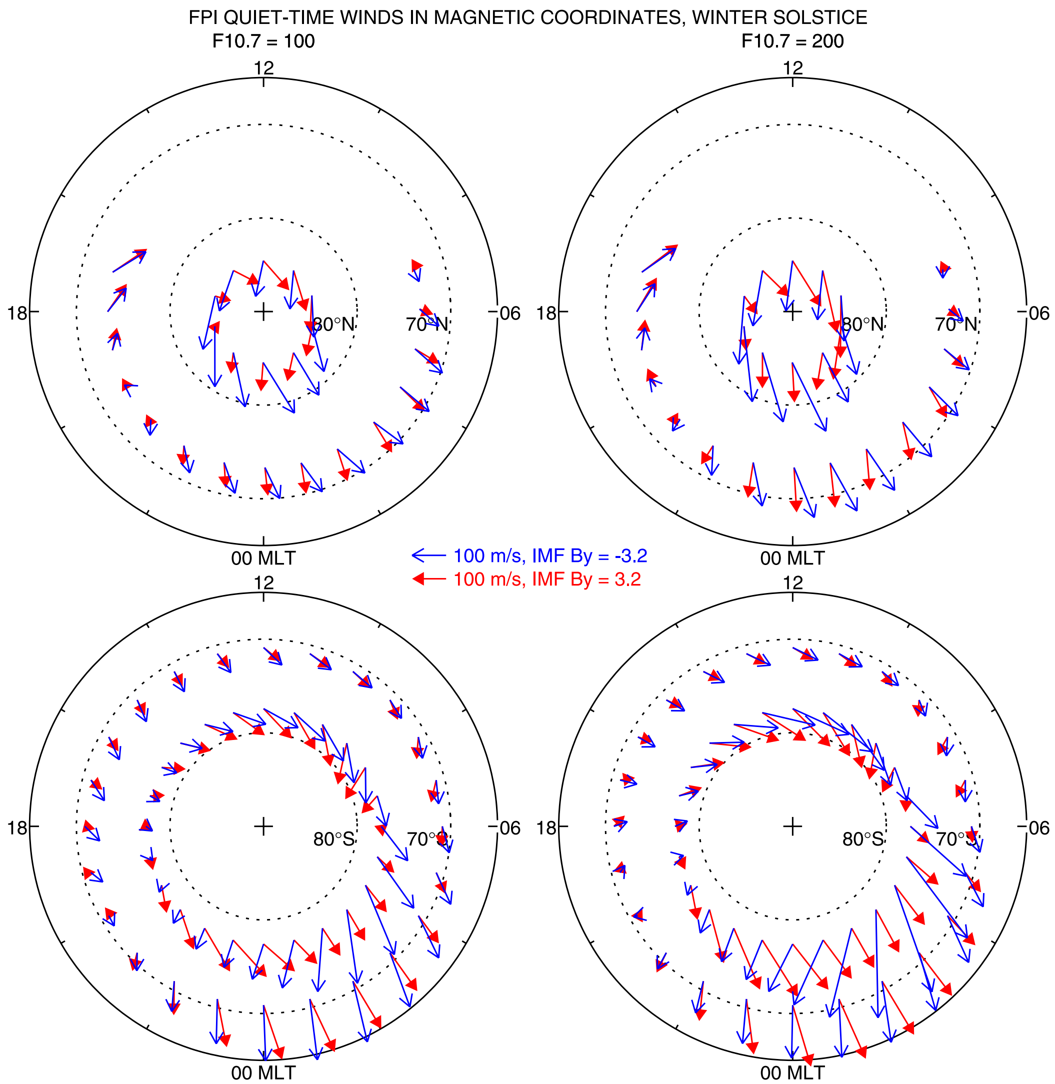

Figure 8. High-latitude quiet time winter solstice wind fields derived from FPI measurements in the (top) northern and (bottom) southern hemispheres. Results are shown for (left) low and (right) high solar EUV conditions, with negative (blue) and positive (red) IMF B_y conditions superimposed. In the northern hemisphere, results from Søndre Strømfjord (outer ring) and Thule (inner ring) are shown. In the southern hemisphere, results from the South Pole FPI are shown. Note that on the sunward side, the Søndre Strømfjord model is constrained to have no B_y dependence (due to a relative lack of data near the dayside terminator), and the results in this local time sector are therefore omitted.

toward the dawn sector. This north/south asymmetry in the B_y effect occurs in the statistical ionospheric convection patterns derived by *Papitashvili and Rich* [2002] and is caused by the interaction of the IMF with the opposite polarities of the northern and southern geomagnetic fields [*Heppner*, 1972].

[23] The differences in direction between the B_y+ and B_y− winds shown in Figure 8 generally appear to be the same for low and high solar EUV conditions. This indicates that the increasing effect of B_y with increasing $F_{10.7}$ is roughly proportional to the overall increase in the wind magnitudes.

3.3. IMF B_y Effects Over Millstone Hill and Halley

[24] IMF B_y influences on the Millstone Hill winds are generally undetectable, but during summer the postmidnight summer zonal winds show a strong dependence on B_y, as shown in Figure 9. The 1-hour response times discussed in section 2.2 are also observed at Millstone Hill, although in this case the peak response time is even less well defined. Also, the data weakly suggest that close to dawn the response broadly maximizes at a time lag of 2–3 hours, rather than 1 hour. For consistency, however, the averages shown in Figure 9 were obtained using a time lag of 1 hour.

[25] The B_y+ winds shown in Figure 9 are up to 50 m/s more westward than the B_y− winds, and the effect diminishes from the north-looking results to the lower-latitude south-looking results. Figure 10 shows the B_y+ and B_y− vector wind patterns over Millstone Hill. The effect appears similar to that of the winter Søndre Strømfjord winds shown in Figure 8 and is again consistent with the direction of the antisunward jet in the convection patterns of *Ruohoniemi and Greenwald* [2005]. However, the fact that the difference

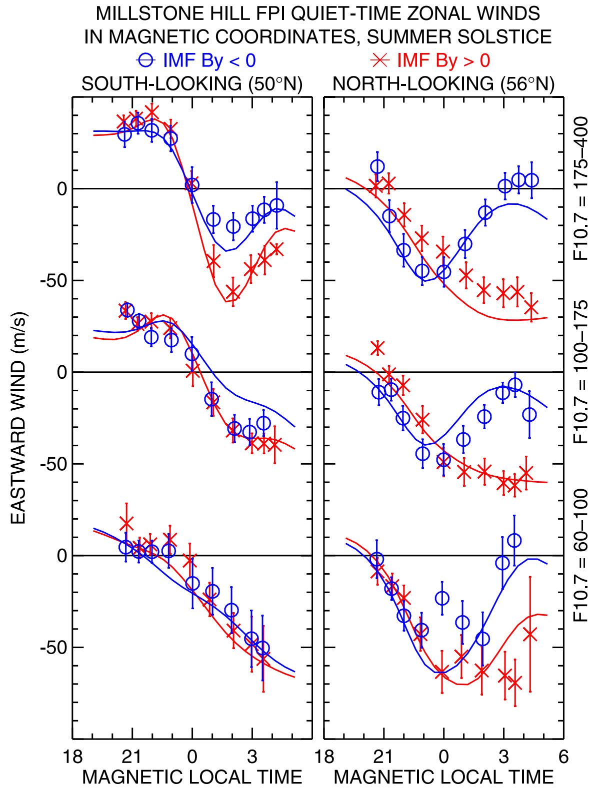

Figure 9. Average quiet time zonal winds over Millstone Hill during summer, with results from negative (blue circles) and positive (red crosses) IMF B_y conditions superimposed. South-looking (north-looking) results are shown on the left (right), and results from a different $F_{10.7}$ bin are shown in each row. The vector winds were converted to magnetic directions, and the zonal wind data were then averaged in 2-hour magnetic local time bins, overlapping at 1-hour intervals. Error bars denote the estimated uncertainty of the mean. The smooth curves show corresponding results from the empirical models.

is largest near dawn possibly suggests that it is a consequence of the stronger dawn cell under summer B_y- conditions [*Ruohoniemi and Greenwald*, 2005; *Papitashvili and Rich*, 2002].

[26] At Halley, we found that IMF B_y effects are very small during the austral winter. This is not inconsistent with the Millstone Hill results (at a slightly lower magnetic latitude), which only show a consistent B_y dependence during summer.

3.4. Quiet Time IMF B_z Effects Over Thule

[27] Under the quiet conditions we consider in this paper, we found that the influences of IMF B_z and B_x are weak and that the winds are most responsive to B_y. Over the polar cap station of Thule, however, B_z does substantially affect the average winds, with weaker antisunward winds for B_z+ conditions, consistent with earlier results [*McCormac et al.*, 1991; *Niciejewski et al.*, 1994]. We therefore included B_z terms in the Thule model, with the B_z values shifted by 1 hour; like the B_y response, the B_z response of the quiet time Thule winds maximizes at a time lag of 1 hour.

[28] Figure 11 illustrates the effect of B_z on the quiet time Thule winds. The top panel shows the vector winds from the empirical model for B_z = –2.0 nT and B_z = +2.5 nT conditions. These values are roughly the average B_z for B_z < 1 and B_z > 1, respectively, under quiet conditions (during which the overall average B_z is ∼1 nT). The winds are substantially more antisunward under B_z- conditions, and the effect appears most pronounced in the noon, dusk, and dawn sectors, where the average wind magnitudes are about three times stronger for B_z-. The bottom panel of Figure 11 shows the antisunward wind component (averaged over local time) continuously as a function of B_z. The circles are binned averages obtained directly from the data, and the solid line shows corresponding results from the empirical model. The data indicate that the response of the quiet time winds to B_z is approximately linear.

4. Conclusion

[29] Using ground-based measurements from seven northern and southern hemisphere stations, we have analyzed climatological patterns of high-latitude quiet time neutral winds in the nighttime upper thermosphere. Our results extend previous analyses of high-latitude wind circulation and constitute the first attempt to empirically model these winds continuously as a function of local time, solar activity, and IMF. To analyze the IMF dependence, we used a proxy derived from ground-based magnetometer measurements; we found that the winds are slightly more sensitive to the ground-based proxy than to space-based IMF measurements.

[30] The signature of duskside anticyclonic ionospheric circulation is evident in the northern hemisphere winds, but in the southern hemisphere, quiet time duskside winds are strongly antisunward over Halley, Antarctica (72°S magnetic) during winter, in apparent disagreement with patterns derived from summer satellite wind measurements.

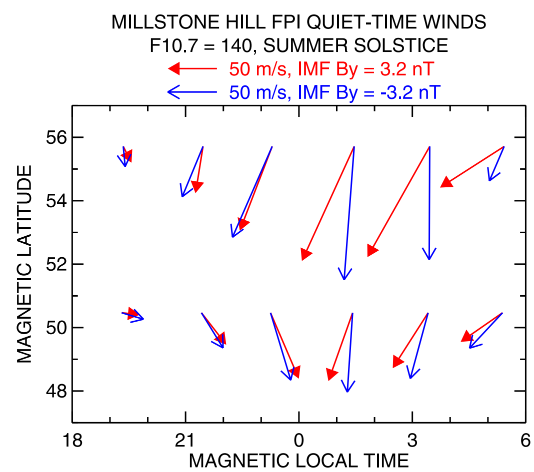

Figure 10. Quiet time wind pattern over Millstone Hill during summer solstice, for negative (blue) and positive (red) IMF B_y conditions. Results are shown for moderate ($F_{10.7}$ = 140) solar EUV conditions. The top and bottom rows of arrows correspond to north- and south-looking observations, respectively.

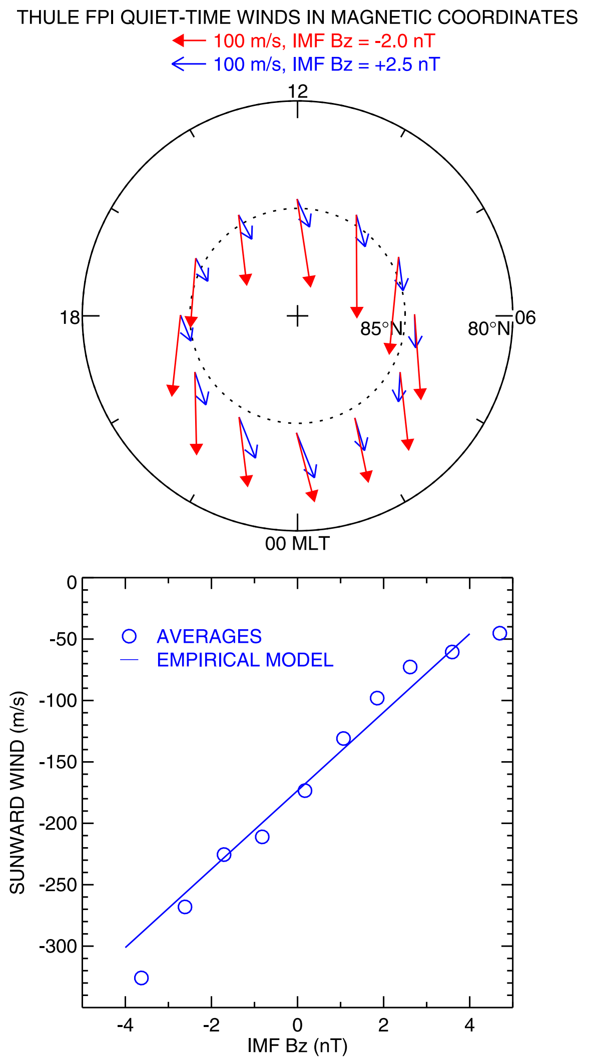

Figure 11. (top) Quiet time wind field over Thule from the empirical model, for IMF $B_z < 1$ (red) and IMF $B_z > 1$ (blue) conditions. In evaluating the model, $F_{10.7}$ was set to 185, the average value for the dataset. (bottom) Antisunward winds, averaged over magnetic local time, as a function of IMF B_z (as represented by the ground based proxy described in section 2.1). The circles show average winds derived directly from the data by binning the geographic northward and eastward winds as a function of local solar time and B_z (2 nT bins at 1 nT intervals), obtaining the sunward component in magnetic coordinates, and re-averaging over local time. The solid line shows corresponding results from the empirical model.

[31] The observed wind speeds generally increase with solar EUV irradiance, except over Millstone Hill (the lowest latitudes considered here, at 53°N magnetic), where the winter wind speeds decrease substantially with increasing EUV. In the midnight local time sector, the solar maximum winds tend to be oriented more westward, compared to solar minimum.

[32] Winds speeds are generally stronger during equinox than during winter, particularly over the South Pole in the direction of eastern longitudes. Nightside winds are generally directed slightly more westward during equinox, compared to winter.

[33] The effect of IMF B_y on the wind patterns resembles its effect on statistical ionospheric convection patterns. In the midnight sector, the northern hemisphere antisunward jet over the polar cap is oriented more toward the dusk (dawn) side when B_y is positive (negative). This effect is reversed in the southern hemisphere, consistent with the opposite polarity of the geomagnetic field relative to the IMF. The response of the winds to B_y increases with $F_{10.7}$, roughly in proportion to the increased wind speeds.

[34] We detected IMF B_y effects in the winds over Millstone Hill, a station that is ordinarily equatorward of the quiet time auroral oval. During summer only, the postmidnight zonal winds over Millstone Hill are more westward when B_y is positive, compared to B_y negative conditions.

[35] Finally, we found that under quiet time conditions, the effects of IMF B_z on the winds are negligible except over the magnetic polar cap station of Thule, where average antisunward wind magnitudes decrease substantially with increasing B_z.

[36] **Acknowledgments.** J. T. Emmert was supported by the National Science Foundation (Aeronomy Program, award ATM-0407823). The FPI wind data and the Quasi-Dipole Coordinate model were obtained from the NSF-supported CEDAR database at the National Center for Atmospheric Research. The magnetic observatory data was provided by Ecole et Observatoire des Science de la Terre and the Danish Meteorological Institute through WDC C1 for Geomagnetism in Copenhagen. The investigations associated with the University of Washington were supported in part by grants OPP-0229251 and ATM-010935 from the National Science Foundation. Zuyin Pu thanks the reviewers for their assistance in evaluating this paper.

References

Crickmore, R. I. (1994), Mean thermospheric winds observed from Halley, Antarctica, *Ann. Geophys.*, *12*, 1101–1113.

Emmert, J. T., M. L. Faivre, G. Hernandez, M. J. Jarvis, J. W. Meriwether, R. J. Niciejewski, D. P. Sipler, and C. A. Tepley (2006), Climatologies of nighttime upper thermospheric winds measured by ground-based Fabry-Perot Interferometers during geomagnetically quiet conditions: 1. Local time, latitudinal, seasonal, and solar cycle dependence, *J. Geophys. Res.*, *111*, A12302, doi:10.1029/2006JA011948.

Heppner, J. P. (1972), Polar-cap electric field distributions related to the interplanetary magnetic field direction, *J. Geophys. Res.*, *77*, 4877–4887.

Heppner, J. P., and N. C. Maynard (1987), Empirical high-latitude electric field models, *J. Geophys. Res.*, *92*, 4467–4489.

Hernandez, G., F. G. McCormac, and R. W. Smith (1991), Austral thermospheric wind circulation and interplanetary magnetic field orientation, *J. Geophys. Res.*, *96*, 5777–5783.

Killeen, T. L., R. A. Heelis, P. B. Hays, N. W. Spencer, and W. B. Hanson (1985), Neutral motions in the polar thermosphere for northward interplanetary magnetic field, *Geophys. Res. Lett.*, *12*, 159–162.

Killeen, T. L., Y.-I. Won, R. J. Niciejewski, and A. G. Burns (1995), Upper thermosphere winds and temperatures in the geomagnetic polar cap: Solar cycle, geomagnetic activity, and interplanetary magnetic field dependencies, *J. Geophys. Res.*, *100*, 21,327–21,342.

McCormac, F. G., and R. W. Smith (1984), The influence of the interplanetary magnetic field Y component on ion and neutral motions in the polar thermosphere, *Geophys. Res. Lett.*, *11*, 935–938.

McCormac, F. G., T. L. Killeen, E. Gombosi, P. B. Hays, and N. W. Spencer (1985), Configuration of the high-latitude thermospheric neutral circulation for IMF B_y negative and positive, *Geophys. Res. Lett.*, *12*, 155–158.

McCormac, F. G., T. L. Killeen, J. P. Thayer, G. Hernandez, C. R. Tschan, and J.-J. Ponthieu (1987), Circulation of the polar thermosphere during geomagnetically quiet and active times as observed by Dynamics Explorer 2, *J. Geophys. Res.*, *92*, 10,133–10,139.

McCormac, F. G., T. L. Killeen, and J. P. Thayer (1991), The influence of IMF B_y on the high-latitude thermospheric circulation during northward IMF, *J. Geophys. Res.*, *96*, 115–128.

McHarg, M., F. Chun, D. Knipp, G. Lu, B. Emery, and A. Ridley (2005), High-latitude Joule heating response to IMF inputs, *J. Geophys. Res.*, *110*, A08309, doi:10.1029/2004JA010949.

Meriwether, J. W., Jr., and P. Shih (1987), On the nighttime signatures of thermospheric winds observed at Sondrestrom, Greenland, as correlated with interplanetary magnetic field parameters, *Ann. Geophys.*, *5A*, 329–336.

Meriwether, J. W., J. P. Heppner, J. D. Stolarik, and E. M. Wescott (1973), Neutral winds above 200 km at high latitudes, *J. Geophys. Res.*, *78*, 6643–6661.

Merriwether, J. W., Jr., T. L. Killeen, F. G. McCormac, and A. G. Burns (1988), Thermospheric winds in the geomagnetic polar cap for solar minimum conditions, *J. Geophys. Res.*, *93*, 7478–7492.

Mikkelsen, I. S., and M. F. Larsen (1983), An analytic solution for the response of the neutral atmosphere to the high-latitude convection pattern, *J. Geophys. Res.*, *88*, 8073–8080.

Niciejewski, R. J., T. L. R. Killeen, and Y. Won (1994), Observations of neutral winds in the polar cap during northward IMF, *J. Atmos. Terr. Phys.*, *56*, 285–295.

Papitashvili, V. O., and F. J. Rich (2002), High-latitude ionospheric convection models derived from Defense Meteorological Satellite Program ion drift observations and parameterized by the interplanetary magnetic field strength and direction, *J. Geophys. Res.*, *107*(A8), 1198, doi:10.1029/2001JA000264.

Rees, D., T. J. Fuller-Rowell, R. Gordon, and M. F. Smith (1986), A theoretical and empirical study of the response of the high latitude thermosphere to the sense of the "Y" component of the interplanetary magnetic field, *Planet. Space Sci.*, *34*, 1–40.

Richmond, A. D. (1995), Ionospheric electrodynamics using Magnetic Apex Coordinates, *J. Geomagn. Geoelectr.*, *47*, 191–212.

Richmond, A. D., and S. Matsushita (1975), Thermospheric response to a magnetic substorm, *J. Geophys. Res.*, *80*, 2839–2850.

Richmond, A. D., C. Lathuillere, and S. Vennerstroem (2003), Winds in the high-latitude lower thermosphere: Dependence on the interplanetary magnetic field, *J. Geophys. Res.*, *108*(A2), 1066, doi:10.1029/2002JA009493.

Ridley, A. J., G. Lu, C. R. Clauer, and V. O. Papitashvili (1998), A statistical study of the ionospheric convection response to changing interplanetary magnetic field conditions using the assimilative mapping of ionospheric electrodynamics technique, *J. Geophys. Res.*, *103*, 4023–4039.

Roble, R. G. (1995), Energetics of the mesosphere and thermosphere, in *The Upper Mesosphere and Lower Thermosphere: A Review of Experiment and Theory*, *Geophys. Monogr. Ser.*, vol. 87, edited by R. M. Johnson and T. L. Killeen, pp. 1–21, AGU, Washington, D. C.

Ruohoniemi, J. M., and R. A. Greenwald (2005), Dependencies of high-latitude plasma convection: Consideration of interplanetary magnetic field, seasonal, and universal time factors in statistical patterns, *J. Geophys. Res.*, *110*, A09204, doi:10.1029/2004JA010815.

Sica, R. J., G. Hernandez, B. A. Emery, R. G. Roble, R. W. Smith, and M. H. Rees (1989), The control of auroral zone dynamics and thermodynamics by the interplanetary magnetic field dawn-dusk (Y) component, *J. Geophys. Res.*, *94*, 11,921–11,932.

Smith, R. W., D. Rees, and R. D. Stewart (1988), Southern hemisphere thermospheric dynamics: A review, *Rev. Geophys.*, *26*, 591–622.

Thayer, J. P., and T. L. Killeen (1993), A kinematic analysis of the high-latitude thermospheric neutral circulation pattern, *J. Geophys. Res.*, *98*, 11,549–11,565.

Thayer, J. P., T. L. Killeen, F. G. McCormac, C. R. Tschan, J. J. Ponthieu, and N. W. Spencer (1987), Thermospheric neutral wind signatures dependent on the east-west component of the interplanetary magnetic field for northern and southern hemispheres as measured from Dynamics Explorer-2, *Ann. Geophys.*, *5*, 363–368.

Vennerstroem, S., B. Zieger, and E. Friis-Christensen (2001), An improved method of inferring interplanetary sector structure, *J. Geophys. Res.*, *106*, 16,011–16,020.

Weimer, D. R. (2001), An improved model of ionospheric electric potentials including substorm perturbations and application to the Geospace Environment Modeling November 24, 1996, event, *J. Geophys. Res.*, *106*, 407–416.

J. T. Emmert, E. O. Hulburt Center for Space Research, U. S. Naval Research Laboratory, Code 7643, 4555 Overlook Avenue, SW, Washington, DC 20375, USA. (john.emmert@nrl.navy.mil)

G. Hernandez, Department of Earth and Space Sciences, University of Washington, Box 351310 Seattle, WA 98195-1310, USA.

M. J. Jarvis, British Antarctic Survey, High Cross, Madingley Road, Cambridge, CB3 0ET, UK.

R. J. Niciejewski, Space Physics Research Laboratory, University of Michigan, Ann Arbor, MI 48109, USA.

D. P. Sipler, Haystack Observatory, Massachusetts Institute of Technology, Westford, MA 01886, USA.

S. Vennerstrom, Danish National Space Center, Juliane Maries Vej 30, DK-2100 Copenhagen O, Denmark.